Chromosome Research (2008) 16:743–760
DOI: 10.1007/s10577-008-1224-8

Analysis of meiotic prophase I in live mouse spermatocytes

Meisha A. Morelli[1], Uwe Werling[2], Winfried Edelmann[2], Mark S. Roberson[1] & Paula E. Cohen[1]*
[1]*Department of Biomedical Sciences and Center for Reproductive Genomics, Cornell University, College of Veterinary Medicine, Ithaca, NY 14853, USA; Tel: +1-607-2534301; Fax: +1-607-253449; E-mail: paula.cohen@cornell.edu;* [2]*Department of Cell Biology, Albert Einstein College of Medicine, Bronx, NY 10461, USA*
**Correspondence*

Received 27 March 2008. Received in revised form and accepted for publication by Herbert Macgregor 21 April 2008

Key words: live imaging, meiosis, mouse, spermatocyte, synaptonemal complex

Abstract

Events occurring during meiotic prophase I are critical for the successful production of haploid gametes. Many prophase I events are mediated by a meiosis-specific structure called the synaptonemal complex. To date, the limited knowledge we have about the dynamics of these prophase I events in mice comes from fixed, two-dimensional preparations of meiotic cells making it impossible to study the three-dimensional (3D) arrangement of meiotic chromosomes. The current study involves the development of an imaging system to view prophase I events in live mammalian spermatocytes by generating a transgenic mouse, *Sycp3–Eyfp*^{21HC}, expressing a fluorescently tagged synaptonemal complex protein, SYCP3. Using this live imaging system, the 3D structural arrangement of chromosomes in the different prophase I substages has been characterized in live spermatocytes, and aspects of the 3D architecture of spermatocytes have been observed that would not be possible with existing techniques. Additionally, chromosome movement in prophase I spermatocytes and meiotic progression from pachynema to diplonema were observed following treatment with the phosphatase inhibitor, okadaic acid (OA), which accelerates the progression of cells through late prophase I. These studies demonstrate that the *Sycp3–Eyfp*^{21HC} live imaging system is a useful tool for the study of mammalian prophase I dynamics.

Abbreviations

2D	two-dimensional
3D	three-dimensional
AE	axial element
CE	central element
ES	embryonic stem
EYFP	enhanced yellow fluorescent protein
IF	immunofluorescence
LE	lateral element
OA	okadaic acid
PBS	phosphate-buffered saline
PGK2	phosphoglycerate kinase 2
SC	synaptonemal complex
SYCP3	synaptonemal complex protein 3

Introduction

Events occurring during meiotic prophase I are critical for the successful completion of meiosis and

Electronic supplementary material

The online version of this article (doi: 10.1007/s10577-008-1224-8) contains supplementary material, which is available to authorized users.

the production of viable gametes. These events include recombination, homologous chromosome pairing, and synapsis. Failure to execute such processes correctly can result in missegregation of chromosomes, leading to meiotic disruption, infertility and/or the production of aneuploid gametes, possibly resulting in birth defects (Hassold *et al*. 1995, 1996, Hassold & Hunt 2001).

At the core of these processes is the synaptonemal complex (SC), a prophase I-specific proteinaceous structure that functions as a scaffold and tethers homologues together. The SC plays an important role in regulating and facilitating chromosome condensation, homologous chromosome recognition and pairing, and the establishment, placement, regulation, and resolution of reciprocal recombination events (Zickler & Kleckner 1999, Page & Hawley 2004), all of which are critical to the successful completion of meiosis. In light of how closely tied the SC is to the success of meiosis, studying the SC and the processes it is involved in is essential to understanding meiosis.

The SC is composed of two lateral elements (LEs), which localize along each homologous chromosome, and a central element (CE), which 'zips' the two LEs together to form a complete SC in a process called synapsis. In the absence of a fully formed SC, such as in leptonema when a CE has yet not formed between the LEs, LEs are referred to as axial elements (AEs) (Zickler & Kleckner 1999, Page & Hawley 2004). Prophase I is divided into distinct substages according to the status of the SC components and the degree of synapsis: leptonema, where AEs begin to form in fragments along the chromosomes; zygonema, when the CE begins to form between each LE pair; pachynema, when full synapsis is achieved; and diplonema, when the CE breaks down and the homologues separate, remaining attached only at their sites of reciprocal recombination (chiasmata).

Currently, techniques used to study prophase I progression and events require the fixation and permeabilization of meiocytes and result in the destruction of three-dimensional (3D) nuclear architecture and cell death. Unfortunately, the lack of viable meiotic culture systems, the difficulty of *in vitro* manipulation of the cells, inefficiency in transgene expression, and the lack of appropriate cell lines make live imaging of meiotic cells extremely difficult. *In vivo* meiotic systems so far include *S. cerevisiae* strains expressing ZIP1::GFP fusion protein (White *et al*. 2004, Scherthan *et al*. 2007), which have been used to characterize chromosome movements in pachynema as well as to observe meiotic progression from one stage to the next (Scherthan *et al*. 2007). In the current study, an analogous system for studying meiosis in live mammalian spermatocytes has been created, validated, and characterized. A transgenic mouse was engineered in which mouse synaptonemal complex protein 3 (SYCP3), the principal AE/LE protein in mouse, is tagged with a fluorescent protein, enhanced yellow fluorescent protein (EYFP), and expressed under the control of the human phosphoglycerate kinase (*Pgk2*) promoter. This approach allows visualization of the 3D structural arrangement of AEs/LEs at different prophase I substages, including aspects that are not observable with current 2D techniques. Additionally, it has allowed for the observation of chromosome movement in prophase I spermatocytes and the monitoring of meiotic progression in individual spermatocytes as they are sped through meiosis by treatment with okadaic acid (OA).

Materials and methods

Transgenic construct creation

Mouse *Sycp3* cDNA was subcloned into the Eyfp-N1 vector (BD BioSciences, Palo Alto, CA, USA) containing the human *PGK2* promoter. Although results have varied, the most recent studies show that mouse *Pgk2* is expressed from preleptotene spermatocytes through to post-meiotic round spermatids (McCarrey *et al*. 1992), and the human *PGK2* promoter has been shown to regulate transgene expression in mice in a manner consistent with endogenous mouse *Pgk2* (Robinson *et al*. 1989, Zhang *et al*. 1999). Mouse *Sycp3* cDNA was fused in-frame with the *Eyfp* coding sequence and electroporated into 129Sv/Ev derived embryonic stem (ES) cells. Five neomycin-resistant, transgene-positive clones were screened for transgene copy number by Southern blot. Clones with high (clone 21) and low (clone 22) copy number insertions of the transgene were selected for injection into C57/Bl6/J blastocysts.

Chimeras were bred with C57/Bl6/J mice and all showed germline transmission. Transgene-positive mice derived from clones 21 (*Sycp3–Eyfp*^{21HC}) and

22 (*Sycp3–Eyfp*^{22LC}) were bred with littermates and also with mice heterozygous for a null deletion of the *Sycp3* gene (Yuan *et al*. 2000) in order to obtain transgene-positive mice on a *Sycp3*$^{-/-}$ background.

Mice were handled according to institutional guidelines for the humane care and use of experimental animals, and with approval for all studies from the Institutional Animal Care and Use Committee at Cornell University. Mice were fed *ad libitum* with standard chow and water and housed under conditions of controlled light (12 h/12 h light/dark cycle) and temperature (27°C).

Southern blot analysis

To assess integrated copy number, ES cell DNA from five positive clones (7, 15, 16, 21, 22) was subjected to Southern blot analysis alongside copy number standards for 1 to 50 copies of the transgene per genome. These standards were made by spiking ES cell DNA from a transgene-negative line with the appropriate amount (1 copy per genome = 0.2 pg per 200 ng genomic DNA) of 6.3 kb EYFP–N1 vector containing the transgene. The α^{32}-P-labeled probe was made by PCR amplification of exons 5 and 6 of mouse *Sycp3*.

Western blot analysis

Equal amounts of whole testis and whole seminal vesicle protein from *Sycp3–Eyfp*^{21HC} and *Sycp3–Eyfp*^{22LC} mice were resolved by SDS-PAGE using a 12% acrylamide gel and transferred to PVDF membrane. The primary antibody used was affinity-purified rabbit anti-SYCP3 antibody (AE763(PB3) (Kolas *et al*. 2005b), 1:1000) and the secondary antibody was horseradish peroxidase-conjugated goat anti-rabbit antibody (1:10 000).

Live imaging and image analysis

Mouse testes were removed under sterile conditions and placed in phosphate-buffered saline (PBS) with 5× penicillin–streptomycin. The testes were decapsulated and washed in fresh PBS with 5× penicillin–streptomycin before being placed in 1 ml of supplemented medium. A modified version of Wiltshire *et al*.'s media recipe (Wiltshire *et al*. 1995) was used: Hepes (25 mM) buffered DMEM culture medium without phenol-red (Invitrogen, Carlsbad, CA, USA) was supplemented with 25 mM $NaHCO_3$, 5% w/v fetal bovine serum (Invitrogen), 1 mM sodium pyruvate (Invitrogen), 10 mM sodium lactate (Sigma, St Louis, MO, USA), and 1× penicillin–streptomycin (Invitrogen).

Tubules were dissociated and large pieces of tubule were removed. Cells were pelleted (1000 *g* for 2 min), resuspended at 2.6×10^6 cells/ml in supplemented medium, and kept in cell culture dishes or plates at 32°C / 5% CO_2 until imaging experiments were performed.

To stain heterochromatin in live cells, Hoechst 33342 (Molecular Probes, Eugene, OR, USA) was added to a final concentration of 0.1 μg/ml and cells were incubated for 5 min at room temperature. Cells were pelleted (1000 *g* for 2 min) and resuspended in the same volume of fresh supplemented DMEM.

A viability assay using trypan blue exclusion was performed immediately after the cells were prepared for imaging and after 6 h in culture. To perform the assay, 10 μl of cell suspension was added to 440 μl PBS and 50 μl trypan blue solution (0.4% trypan blue in PBS, 10× stock). The number of stained and unstained cells was then counted using a hemocytometer and the ratio was used to determine cell viability. Importantly, the viability of the cells, both those treated with Hoechst and those left untreated, was 80–90% at the time of plating and after 6 h of incubation was 70–75%, indicating that cells remain viable throughout our visualization and culture procedures.

For live imaging, either a 100 μl aliquot of germ cell suspension was placed in a 35 mm glass-bottomed microwell dish (MatTek, Ashland, MA, USA) or cells were embedded in fibrinogen clots, as described below. This latter technique was employed when cells were to be sequentially imaged, allowing for repeatable location of the same cell with successive microscope sessions. Images were obtained using an Axiovert 200M (Carl Zeiss Inc., Gottingen, Germany) and the cells were incubated at 32°C / 5% CO_2 during the entire imaging period, which varied in length but lasted no longer than 6 h. Z-stack images were obtained with the fluoarc lamp at 70% intensity and a 0.25 μm distance between optical sections. Exposures were taken in the YFP (50–200 ms) channel and sometimes the DAPI (1–5 ms), CFP (125 ms) and DIC (1–5 ms) channels. For the leptotene and early zygotene spermatocytes, which do

not have visible EYFP signal, 2D images were taken in the DIC, YFP, and DAPI channels by snapping images using the live window. The filter sets used were: YFP (46HE), DAPI (49), CFP (47HE). See http://www.zeiss.com/micro for additional information. Axiovision v4.6 was used to deconvolve images and render them into 3D.

For time-lapse imaging, fibrinogen-immobilized spermatocytes were imaged in the YFP channel in a single focal plane. Images were taken at rates from around 1 per second to one every 30 seconds over periods of 5 min to 2 h.

For some images, the Zeiss structured illumination system (Apotome), which requires a longer exposure time but gives higher-resolution images, was used instead of deconvolution. For Apotome images the exposure time was increased to between 500 and 800 ms for the YFP channel and the distance between optical sections was increased to 0.5 or 0.75 μm.

Cells were staged as described using the criteria outlined in the results. AE/LE measurements were made using the 3D measurements function in the Zeiss Axiovision v4.6 software. Only AEs/LEs which could be tracked unambiguously along their entire length were measured. The thickening of the AEs/LEs at the chromosome ends (sites of nuclear envelope attachment) was often used to help identify the ends of the AE/LE. The clipping function was also used to track AEs/LEs around the interior of the 3D structure of the nucleus.

Fibrinogen clots and immunostaining

A modified version of the oocyte fibrinogen clot procedure (Hunt *et al*. 1995) was used for spermatocytes. This procedure fixes cells in 3-dimensional space, allowing them to be visualized repeatedly over successive microscope sessions. A germ cell suspension in supplemented DMEM medium was obtained from *Sycp3–Eyfp*^{21HC} mice. The cells were pelleted (1000 *g* for 2 min) and resuspended in 10–20 μl of fibrinogen (0.005 g of bovine plasma fibrinogen from Calbiochem (La Jolla, CA, USA), dissolved in 400 μl supplemented DMEM media). This suspension was spread onto a 35 mm glass-bottomed dish (MatTek) with a reference and orientation point marked. An amount of bovine plasma thrombin (Sigma) equivalent to the amount of fibrinogen was added to each dish to set the clot. The cells were imaged, as described above, in supplemented DMEM and their positions were recorded using the 'mark and find' function in the Axiovision v4.6 software. Immediately after imaging, the clots were fixed for 5 min in 4% paraformaldehyde (containing 2% Triton X-100) and blocked for 30 min in 0.1% normal goat serum in PBS at 37°C and 30 min in 10% normal goat serum in PBS (containing 0.1% Triton X-100 and 0.02% sodium azide) at 37°C. Immunofluorescence was performed as described below for meiotic spreads. The clots were again imaged at the previously marked positions. Z-stack images were taken in the GFP (30 ms, Filterset 38HE), CY5 (200 ms, Filterset 26), DIC (5 ms), and DAPI (5 ms, Filterset 49) channels with the fluoarc lamp at 100% intensity and 0.25 μm distance between optical sections. For leptotene and early zygotene spermatocytes, two-dimensional (2D) images were taken in the DIC, GFP, CY3 (Filterset 20), and DAPI channels by snapping images using the live window. Images of the same spermatocyte before and after immunofluorescence (IF) were matched for comparison.

Chromosome preparations and immunofluorescent staining

Chromosome preparations and immunofluorescence were performed as described previously (Peters *et al*. 1997, Kolas *et al*. 2005a). Primary antibodies used were rabbit anti-mouse SYCP1 (SYN1, 1:500), mouse anti-mouse SYCP3 (mpc2003, 1:5000), CREST human autoimmune serum (1:5000) to detect centromeres, mouse γH2AX (1:20 000, Millipore, Billerica, MA, USA) to aid in staging spermatocytes and rabbit anti-mouse SMC3 (Eijpe *et al*. 2003). Secondary antibodies used were Alexafluor 488 goat anti-rabbit, Alexafluor 555 goat anti-mouse, and Alexafluor 647 goat anti-human (1:500, Invitrogen).

Fluorescence recovery after photobleaching

Germ cells embedded in fibrinogen clots (20 μl total volume, 2.5×10^6 cells/ml) were imaged as described above. After imaging, the aperture on the microscope was closed so that only a small area of the viewing field was exposed to light. A target cell was positioned either entirely or partially in the exposed portion of the field and was photobleached using a dichroic mirror filter (2–3 min). The cells were imaged immediately after photobleaching and after 24 h of incubation (32°C / 5% CO_2).

OA treatment of spermatocytes from Sycp3–Eyfp^{21HC} mice

The procedure for treatment with OA was modified from Wiltshire *et al*. (1995). 100 μl of a 2.5×10^6 cells/ml germ cell suspension in supplemented DMEM media was prepared as described previously. This suspension was placed in a glass-bottomed microwell dish (MatTek) and OA was added to a final concentration of 5 μm. The dish was incubated at 32°C / 5% CO_2 in the incubation chamber on the Axiovert 200 M. Images were taken immediately after addition of OA and after 6 h of incubation. Time-lapse imaging was also performed on OA-treated spermatocytes. Okadaic acid was added to the media as described above and spermatocytes were imaged in a single focal plane over 6 h, with an image being taken every 5 min.

Results

Creation of Sycp3–Eyfp^{21HC} and Sycp3–Eyfp^{22LC} transgenic mouse lines

The *Sycp3–Eyfp* construct driven by the human *PGK2* promoter was electroporated into ES cells (Figure 1a) and Southern blot analysis was used to detect endogenous *Sycp3* signal and to estimate transgene copy number (Figure 1b). ES cell lines 21 and 22 were picked for blastocyst injection (Figure 1b, asterisks) and two transgenic mouse lines were

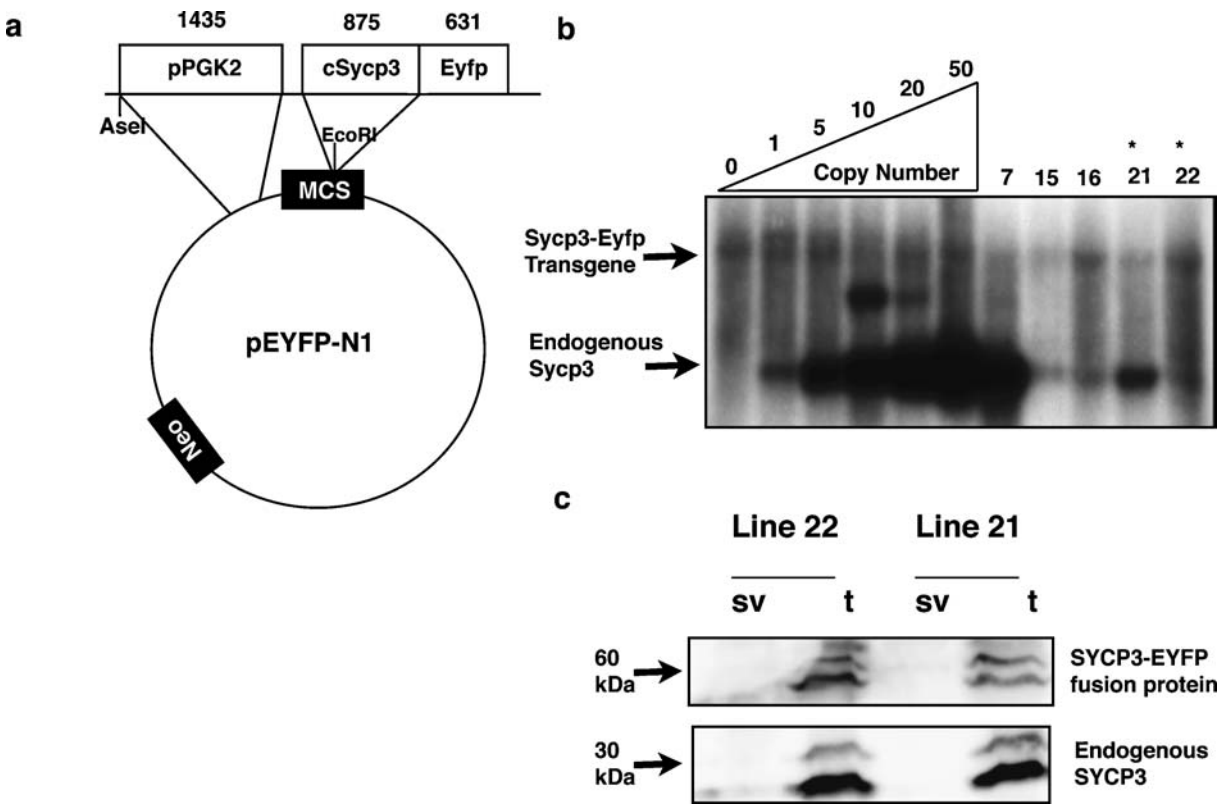

Figure 1. Creation and validation of the *Sycp3–Eyfp* transgenic mouse lines. (**a**) Construct map. A diagram of the transgenic construct electroporated into mouse blastocysts. (**b**) Copy number determination. Southern blot analysis of 5 μg genomic DNA from ES cell lines with transgene insertions (determined by PCR) alongside copy number standards made from 5 μg genomic DNA from wild-type ES cell lines spiked with appropriate (1 copy per genome = 0.2 pg per 200 ng genomic DNA) of 6.3 kb EYFP-N1 vector containing the transgene. The probe used was made from exons 5/6 of *Sycp3* cDNA. The asterisks indicate the low and high copy number lines selected for blastocyst injection. (**c**) Western blot analysis of protein extracts from testis (t) and seminal vesicle (sv) of *Sycp3–Eyfp^{21HC}* and *Sycp3–Eyfp^{22LC}* mice.

derived, a high-copy-number line (*Sycp3–Eyfp*^{21HC}) and a low-copy-number line (*Sycp3–Eyfp*^{22LC}).

Transgene propagation in the expected ratios was confirmed by PCR (data not shown). Both *Sycp3–Eyfp*^{21HC} and *Sycp3–Eyfp*^{22LC} male and female mice are viable and fertile with normal meiotic progression, as assayed by meiotic spreads and their ability to fertilize, indicating that transgene expression does not disrupt the meiotic process or wild-type SYCP3 function.

Western blot analysis demonstrates co-expression of the fusion and endogenous protein in the expected tissues (seminiferous epithelium), and confirms their absence in other tissues (seminal vesicles) (Figure 1c). This is consistent with the testis-specific expression previously described for human *PGK2*-driven transgenes (Robinson *et al*. 1989). Testis protein from *Sycp3–Eyfp*^{21HC} and *Sycp3–Eyfp*^{22LC} mice show doublet bands at 30/33 kDa (consistent with endogenous SYCP3 (Lammers *et al*. 1994)) and around 60 kDa (consistent with the 60 kDa size predicted for the SYCP3–EYFP fusion protein).

Initial observation of transgenic spermatocytes shows that EYFP signal is visible and in a pattern consistent with AE/LE localization in both transgenic lines. As expected, oocytes from day 1 *post partum* ovaries did not show any visible fluorescence (not shown). However, the fluorescent signal in the *Sycp3–Eyfp*^{21HC} mice was much more robust than the *Sycp3–Eyfp*^{22LC} mice and thus for all subsequent experiments discussed in this paper only *Sycp3–Eyfp*^{21HC} mice were used. Co-localization of EYFP signal with endogenous SYCP3 was demonstrated by live imaging of fibrinogen-immobilized spermatocytes followed by fixation and immunofluorescence using an anti-SYCP3 antibody (Figure 2). The live EYFP signal is seen to coincide with the SC subsequently identified by immunostaining. Immunostaining without primary antibody produces no

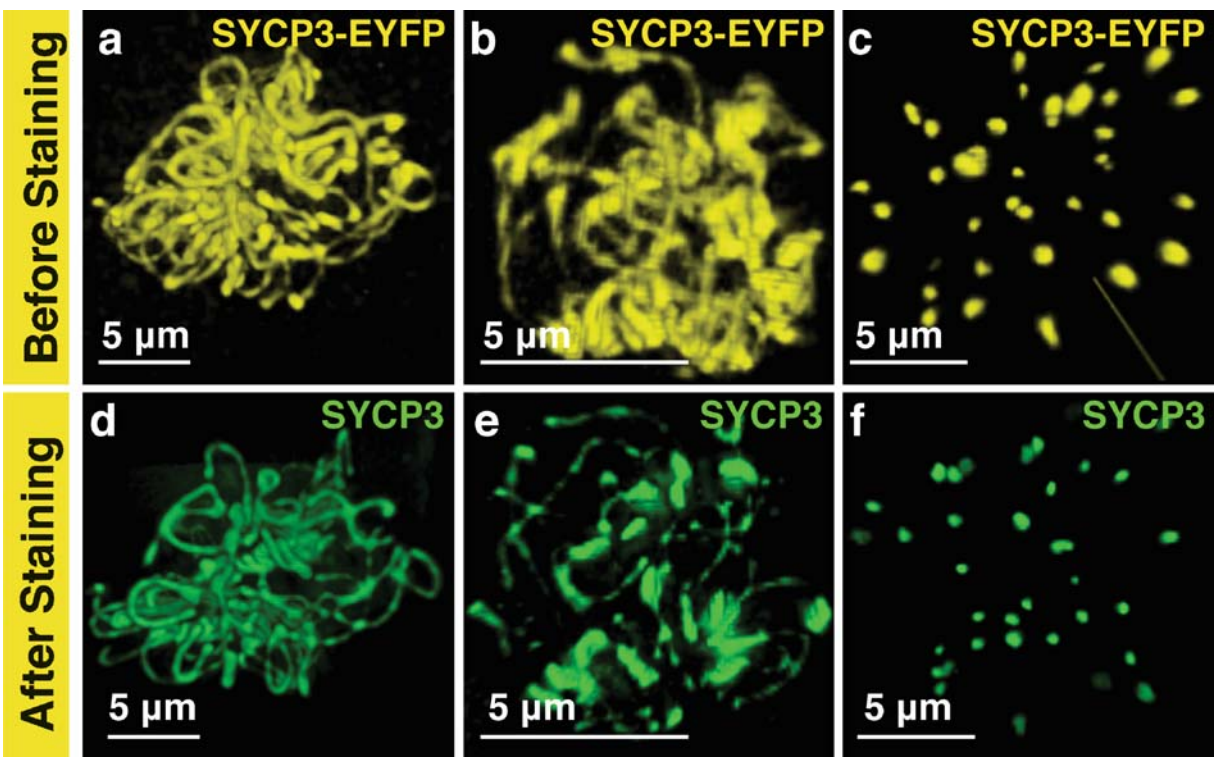

Figure 2. Signal overlap between SYCP3-EYFP and endogenous SYCP3. (**a**, **b**, **c**) 3D renderings of z-stack images in the YFP channel of *Sycp3–Eyfp*^{21HC} spermatocytes in different prophase I substages immobilized in fibrinogen clots before staining to show endogenous EYFP fluorescence. (**d**, **e**, **f**) The same spermatocytes after fixation and immunofluorescence staining to show SYCP3 localization. The spermatocytes in (a), (b), (d) and (e) are in diplonema and the spermatocyte in (c) and (f) is in diakinesis. Scale bars represent 5 µm.

fluorescent signal, demonstrating that the signal seen after fixation was due solely to immunostaining and not to residual SYCP3–EYFP fluorescence (data not shown). Thus, EYFP signal reliably labels AEs/LEs, indicating that the EYFP tag does not interfere with SYCP3 localization.

SYCP3-EYFP transgenic protein expression does not rescue the phenotype of Sycp3$^{-/-}$ mice

Meiotic spreads were prepared from spermatocytes of *Sycp3*$^{-/-}$ *Sycp3–Eyfp*^{21HC} and *Sycp3*$^{-/-}$ *Sycp3–Eyfp*^{22LC} adults and wild-type littermate controls. The spreads were stained for localization of AE/LE (SYCP3) and CE (SYCP1) components of the SC, centromeres, and meiotic cohesins (SMC3).

The presence of the SYCP3-EYFP fusion protein failed to rescue the *Sycp3*$^{-/-}$ phenotype. The transgene-positive *Sycp3*$^{-/-}$ mice exhibit a similar sterile phenotype to the *Sycp3*$^{-/-}$ mice previously described (Yuan *et al*. 2000), with no SCYP3 staining and persistent SYCP1 fragments along the chromosome cores (Figure 3a–c). The presence of intact cohesin-containing chromosome cores, consistent with

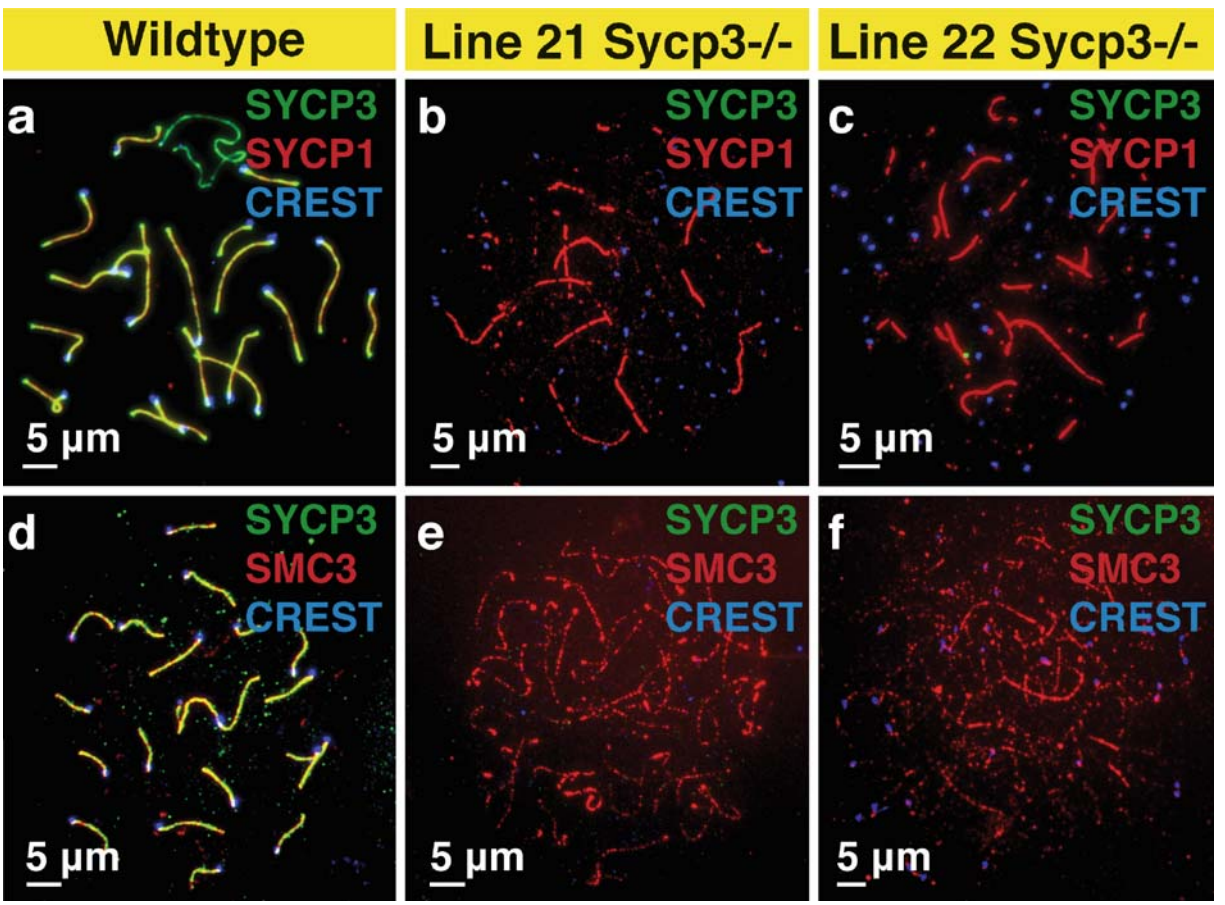

Figure 3. SYCP3–EYFP transgenic protein expression fails to rescue the *Sycp3* null phenotype. (**a**) Wild-type mouse spermatocyte showing SYCP3 (green), SYCP1 (red) and CREST (blue) staining to show the SC and synapsis. (**b**) *Sycp3*$^{-/-}$ spermatocyte expressing the line 21 transgene (same staining as (a)). (**c**) *Sycp3*$^{-/-}$ spermatocyte expressing the line 22 transgene (same staining as (a)). (**d**) Wild-type mouse spermatocyte showing SYCP3 (green), SMC3 (red) and CREST (blue) staining to show the chromosome cores. (**e**) *Sycp3*$^{-/-}$ spermatocyte expressing the line 21 transgene (same staining as (d)). (**f**) *Sycp3*$^{-/-}$ spermatocyte expressing the line 22 transgene (same staining as (d)). Note that, unlike the wild-type, both the line 21 and line 22 spermatocytes on the *Sycp3*$^{-/-}$ background do not show any SYCP3 staining along the chromosome cores, although they do show fragmented stretches of SYCP1. Additionally, both line 21 and line 22 spermatocytes on the *Sycp3*$^{-/-}$ background show cohesin (SMC3) staining along the cores. This phenotype is identical to *Sycp3*$^{-/-}$ mice with no transgene expression, indicating that transgene expression does not rescue the *Sycp3* null phenotype. Scale bars represent 5 µm.

previous results for *Sycp3*$^{-/-}$ mice (Pelttari *et al.* 2001), was demonstrated by meiotic cohesin SMC3 localization (Figure 3d–f).

Prophase I substages can be discerned in live transgene-positive spermatocytes

The accumulation of AE/LE proteins along the homologous chromosomes and the synaptic state of the tripartite SC define prophase I substages and were used to characterize prophase I substages in SYCP3–EYFP-expressing spermatocytes (Table 1). Synapsis was determined by the continuity and completeness of the AE/LE and the presence and location of regions of unpaired AE in a set of homologues that are otherwise paired, indicating unsynapsed regions. Also, numerous AE/LE-related measurements could be made in live spermatocytes, including AE/LE length, which is measurable from late zygonema to early diplonema. Owing to the manipulation of the spermatocytes in the spreading, fixation and staining procedures as well as the limitations of the live-imaging due to photobleaching, there are noticeable differences between the live spermatocytes (Figure 5, columns 1–3) and the spread spermatocytes (Figure 5, column 4). However, the two preparations are similar enough that we are able to determine the prophase I substage of live spermatocytes even though it is not as straightforward as staging spread spermatocytes.

In live leptotene and early zygotene cells, identified by Hoechst staining and further aided by cell diameter, distinct AE fragments cannot be observed as the endogenous fluorescence is too weak or the transgene is not expressed this early in meiosis

Table 1. Summary of the morphological appearance of prophase I substages, as observed in live mammalian spermatocytes

	Leptonema	Zygonema	Pachynema	Diplonema	Diakinesis
LE formation	AEs are present in fragments, but fluorescence is too weak to observe them in live cells.	AE/LEs in varying degrees of formation and pairing. Sometimes pairing homologues (split at the ends) can be seen.	Fully formed and synapsed LEs. No pairing or splitting homologues can be seen. The XY body can sometimes be seen separated from the rest of the nucleus.	SC in varying degrees of disassembly, as assessed by AE/LE appearance. Sometimes separating homologues (split in the middle) can be seen.	Punctate SYCP3-EYFP fragments around the nucleus. In some cases, SYCP3-EYFP fragments can be seen lined up in parallel planes in the nucleus. SYCP3-EYFP fragments are located at the centromeres.
Chromatin	Numerous small, diffuse, regions of heterochromatin distributed around the nucleus.	Larger regions of heterochromatin, distributed asymmetrically around the nucleus in many cases, especially in early zygonema.	Generally 5–10 very distinct heterochromatic regions distributed throughout the nucleus.	Similar to chromatin distribution in pachynema.	Numerous small, diffuse regions of heterochromatin distributed around the nucleus, often around SC fragments.
Telomere clustering	Telomere clustering cannot be observed in leptonema.	Telomeres clustered in asymmetrically distributed regions of heterochromatin. The clusters are often larger in earlier zygonema than in later zygonema, pachynema and diplonema.	Telomeres clustered in groups of 2–10. Clusters are distributed more evenly around the nucleus then in zygonema.	Similar to telomere clustering in pachynema.	Residual SYCP3-EYFP fragments are not complete enough to observe telomere clustering.

(Figure 4a–c). However, fragmented AEs/LEs can be observed in immunofluorescently stained spermatocytes in fibrinogen clots (Figure 4g) with the presence of axial γH2AX staining used to confirm the stage (Figure 4f). Cells were also seen that stained strongly with γH2AX but did not have visible AEs, which could be preleptotene spermatocytes. There are conflicting results on when the expression of *Pgk2* is initiated, with some studies indicating that expression starts as late as pachynema (Robinson *et al*. 1989, Thomas *et al*. 1989) and others reporting expression starting in preleptotene spermatocytes (McCarrey *et al*. 1992). There is evidence that transgenes expressed in the mouse under the control of the human *PGK2* promoter do not express until pachynema (Robinson *et al*. 1989) and thus the absence of fluorescence in leptotene nuclei could be explained by the lack of transgene expression rather than the fluorescence being too weak.

Zygotene nuclei display distal regions of unsynapsed AE and/or discontinuous AEs/LEs (Figure 5e–h and Supplementary Movie S1). Pachytene nuclei display LEs that are continuously paired along their length and in later pachynema the chromosomes have thickened ends (indicating nuclear envelope attachment) (Figure 5i–l and Supplementary Movie S2). The live pachytene spermatocyte shown in Figure 5i–k appears to be in late pachynema as the SC ends are somewhat thickened. The spread pachytene nucleus shown in Figure 5l appears to be in mid-pachynema as the chromosomes are highly compacted and there is no thickening of the SC ends. The XY body (Handel 2004) can also be observed separated from the rest of the nucleus (Figure 6a, green arrow, and Supplementary Movie S3) in many pachytene-stage spermatocytes. Nuclei are determined to be in diplonema when regions of unsynapsed AE are observed in the middle of otherwise paired homologues, resulting in the characteristic 'bubbles' that form as the SC breaks down and homologues separate (Figure 5m–p and Supplementary Movie S4). Diplotene nuclei are also characterized by more highly compacted AEs/LEs and more pronounced thickening of the AE/LE ends than pachytene or zygotene nuclei. Diakinesis-stage spermatocytes, have small fragments of SYCP3–EYFP distributed around the nucleus (Figure 5q–t). Previous results indicate that in diakinesis residual SYCP3 fragments are localized to the centromeres (Moens & Spyropoulos 1995). Thus, to further confirm diakinesis stage spermatocytes, CREST autoimmune serum

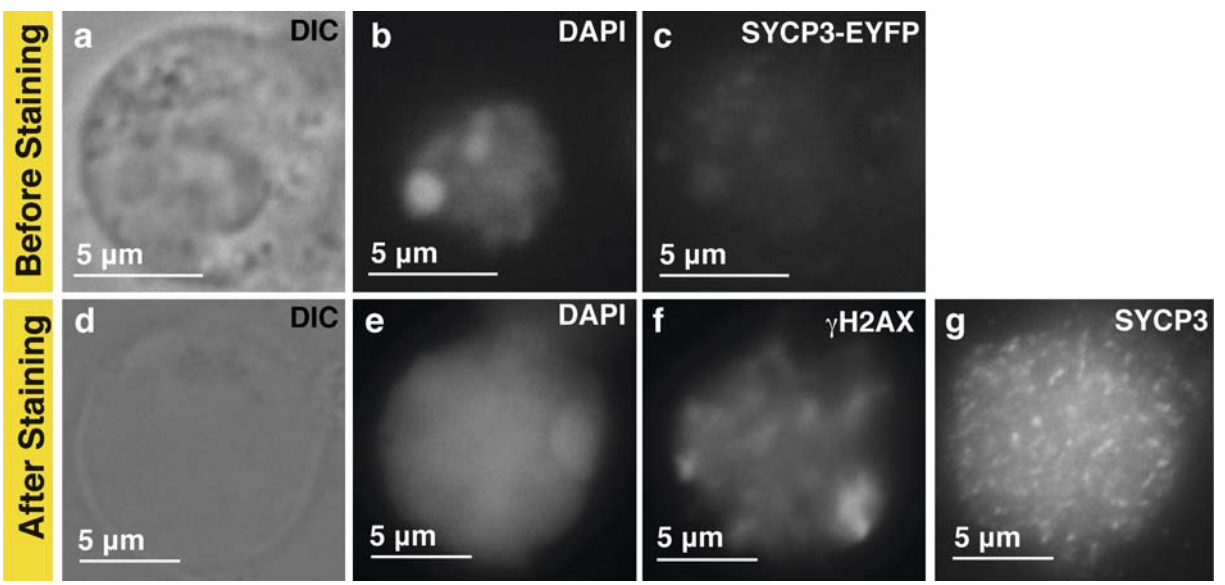

Figure 4. Imaging of leptotene/early zygotene spermatocytes before and after staining. (**a**) A DIC image of a live leptotene or early zygotene spermatocyte, as determined by Hoechst staining and cell diameter. (**b**) A DAPI image of Hoechst staining in the same live spermatocyte in (a). (**c**) A YFP image of the same live spermatocyte in (a). (**d**) A DIC image of a fixed and stained leptotene or early zygotene spermatocyte. (**e**) A DAPI image of the spermatocyte in (d). (**f**) An image of γH2AX staining in the spermatocyte in (d) showing axial staining characteristic of leptonema and zygonema. (**g**) An image of SYCP3 staining of the spermatocyte in (d). Scale bars represent 5 µm.

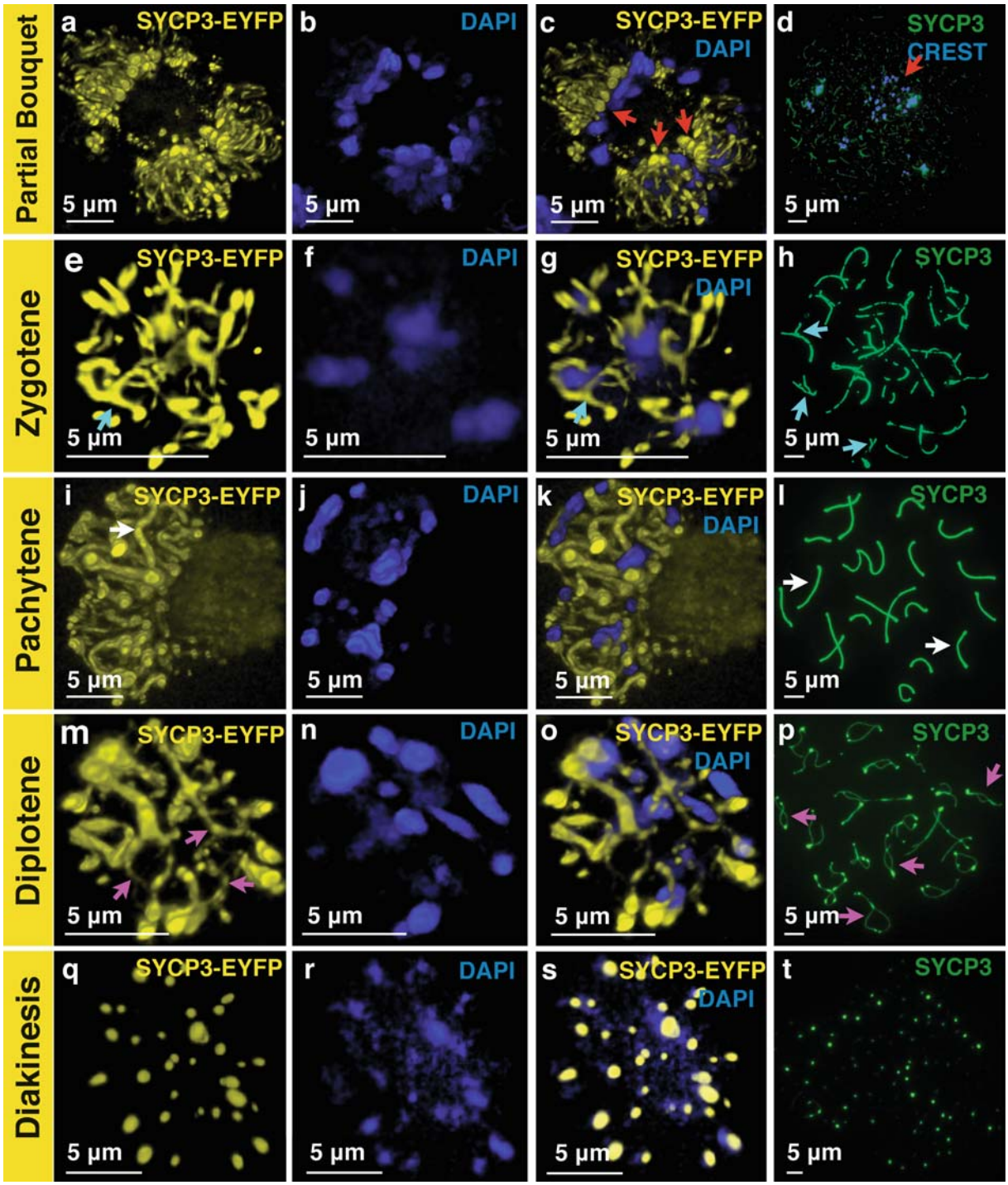

staining was employed. Spermatocytes thought to be in diakinesis from live imaging show complete co-localization between SYCP3–EYFP fragments and centromeres after staining (Figure 7), thus confirming the staging. Furthermore, SYCP3–EYFP fragments in diakinesis spermatocytes are also occasionally observed aligned in parallel planes in the nucleus (Figure 6b and Supplementary Movie S5), indicating the alignment of

◀ *Figure 5*. 3D renderings of z-stack images of spermatocyte nuclei from *Sycp3–Eyfp*^{21HC} spermatocytes at different prophase I substages. Images in the first column (**a**, **e**, **i**, **m**, **q**) were taken in the YFP channel. Images in the second column (**b**, **f**, **j**, **n**, **r**) are the same cells as the first column but images were taken in the DAPI channel. Images in the third column (**c**, **g**, **k**, **o**, **s**) are the merges of the DAPI and YFP channel images. Images in the first row (**a**, **b**, **c**) are of a cluster of four zygotene nuclei in a partial bouquet stage with the telomeres gathered together at one end of the nucleus but not completely in a single tightly clustered bouquet. Images in the second row (**e**, **f**, **g**) are of a zygotene nucleus. Images in the third row (**i**, **j**, **k**) are of a cluster of three nuclei, two of which are in pachynema. Images in the fourth row (**m**, **n**, **o**) are of a diplotene nucleus. Images in the fifth row (**q**, **r**, **s**) are of a nucleus in diakinesis. The last column of images (**d**, **h**, **l**, **p**, **t**) are meiotic spreads from a wild-type (non-transgenic) mouse stained for SYCP3 (green) with immunofluorescence. Spreads are shown as examples of each prophase I stage (d, partial bouquet; h, zygonema; l, pachynema; p, diplonema; and t, diakinesis) and approximately match the stages of the nuclei to the left as a comparison between the two ways of imaging. In the example image of a partial bouquet, CREST staining is also shown in blue to show the clustering of the centromeres. Red arrows point to telomeres clustered in regions of heterochromatin. Light blue arrows point to distal regions of unsynapsed AE. Pink arrows point to chromosomes in which regions of unsynapsed AE are observed in the middle of otherwise paired homologues (creating 'bubbles') as the chromosomes separate from each other in diplonema. White arrows point to LEs that are continuous and paired along the length of the chromosome, typical of completely paired pachytene LEs. Scale bars represent 5 μm.

homologues along the metaphase plate. Telomere clustering and heterochromatin staining (described below) are other criteria used for staging.

Telomere clustering is observed in live fluorescent spermatocytes

Telomere movement in meiosis (Bass *et al*. 1997, Scherthan *et al*. 2000, Tanemura *et al*. 2005, Scherthan 2007), especially the clustering together of telomeres in the highly conserved but transient 'telomere bouquet' stage (Zickler & Kleckner 1998), is thought to play a role in pairing efficiency and recombination (Trelles-Sticken *et al*. 2000, Liu *et al*. 2004). Since proximal telomeres are highly heterochromatic and are easily identifiable at the ends of chromosomes, the visualization of telomere clustering in spermatocytes from *Sycp3–Eyfp*^{21HC} mice was aided by staining of heterochromatin with Hoechst 33342. Identification of telomeres in live cells requires identification of chromosomes marked with SYCP3–EYFP. Thus telomeres cannot be viewed in leptonema as EYFP fluorescence is too weak to observe AEs. However, heterochromatic regions are visible as relatively small, diffuse regions dispersed throughout the nucleus. In zygotene nuclei, telomere clustering is evident and occurs in large heterochromatic regions. These clusters are often concentrated at one end of the nucleus (Figure 5a–d and Figure 6d, red arrows) and partial bouquets are observed occasionally (Figure 5a–d). In later zygotene nuclei, telomere clusters are dispersed more evenly around the nucleus (Figure 5e–h and Figure 6c, red arrows). In pachytene nuclei, telomere clusters retain the more even nuclear distribution observed in late zygotene nuclei but the heterochromatic regions become sharper as chromosomes condense further (Figure 5i–l). Diplotene nuclei retain the distinct heterochromatic regions dispersed throughout the nucleus (Figure 5m–p). This is lost in diakinesis spermatocytes, which have heterochromatic patches only around the residual SYCP3–EYFP at centromeres. The number of telomere clusters throughout prophase I remains constant at 5–10 clusters per nucleus with 2–5 telomeres per cluster. The clusters are distributed around the nuclear periphery. Additionally, consistent with previous findings (Scherthan *et al*. 1996), the telomeres present in the clusters appear to be the proximal, centromere-associated telomeres since the number of CREST signals is equivalent to the number of telomeres in each cluster (data not shown). Distal telomeres are more difficult to identify and thus at this time we cannot conclude whether the distal telomeres are present in clusters or not.

No recovery of SYCP3–EYFP fluorescence is seen after photobleaching

Fluorescence recovery after photobleaching in SYCP3–EYFP-expressing spermatocytes was examined (Figure 8) in order to determine SYCP3 turnover rate and the ability to recover fluorescence, specifically its implications for imaging the same nucleus multiple times. Spermatocytes were imaged and then entire cells (Figure 8a–c and d–f) or portions of cells (Figure 8g–i) were photobleached. The cells were re-imaged immediately and then imaged again 24 h later in order to give the cells ample time to regenerate fluorescence without making cell viability a major

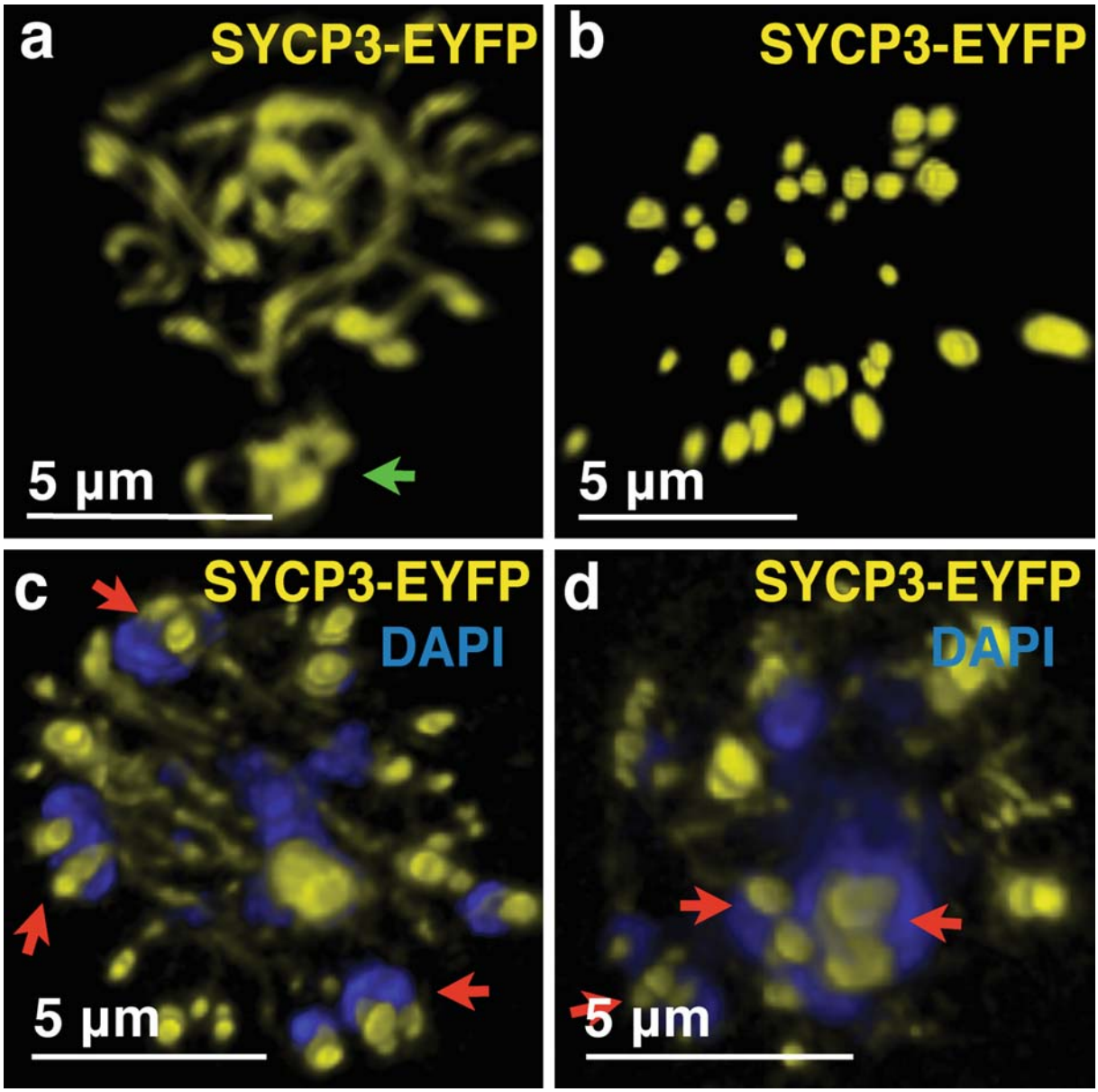

Figure 6. Observations on the 3D architecture of spermatocytes that can be made using fluorescent spermatocytes. (**a**) 3D rendering of a z-stack image of a pachytene spermatocyte from a *Sycp3–Eyfp*^{21HC} mouse imaged in the YFP channel, clearly showing the XY body separated from the rest of the nucleus (green arrow). (**b**) 3D rendering of a z-stack image of a diakinesis stage spermatocyte from a *Sycp3–Eyfp*^{21HC} mouse imaged in the YFP channel, showing the fragments of SYCP3 lined up in parallel planes in the nucleus. (**c**, **d**) 3D renderings of z-stack images of diplotene spermatocytes from a *Sycp3–Eyfp*^{21HC} mouse, stained with Hoechst 33342 and imaged in the YFP and DAPI channels. Telomere clustering is indicated by the red arrows. Scale bars represent 5 µm.

issue. After 24 h the cells still appeared viable and in the partially bleached cells the half that was not bleached was still fluorescent (Figure 8c,f), but no recovery of fluorescence was observed beyond minor redistribution through the nucleus (Figure 8c,f), indicating subtle movement of chromosomes. In the cells that were completely photobleached (Figure 8g–i), no recovery of fluorescence was seen. This indicates

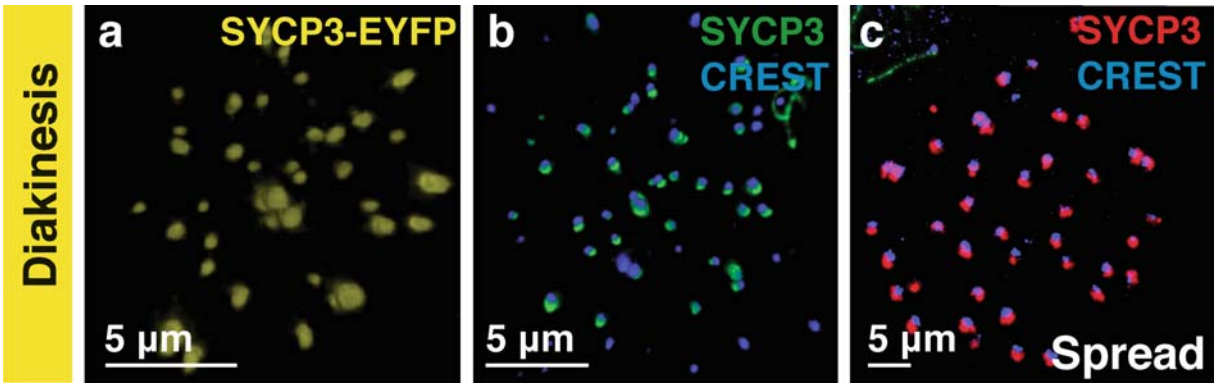

Figure 7. Overlap of residual EYFP signal with centromeres in diakinesis stage spermatocytes. (**a**) A 3D rendering of a z-stack image of a diakinesis stage spermatocyte taken in the YFP channel before fixation and staining. (**b**) A 3D rendering of a z-stack image of the same diakinesis spermatocyte fixed and stained with IF for SYCP3 (green) and CREST (blue). (**c**) A meiotic spread of a diakinesis stage spermatocyte stained with IF for SYCP3 (green) and CREST (blue) shown for comparison purposes. Scale bars represent 5 μm.

that there is very little, if any, turnover of SYCP3 protein, and implies that the SC is a very stable structure once formed.

Subtle movements of chromosome ends are observed in Sycp3–Eyfp^{21HC} spermatocytes

Sycp3–Eyfp^{21HC} spermatocytes observed for periods of 5–180 min display subtle, but continuous, movements of the ends of chromosomes (Supplementary Movies S6–S10). Movement was seen in chromosomes in zygonema through diplonema, but not diakinesis. Chromosomes in some cells appear to move quite rapidly, while others appear to move much more slowly. For example, gross chromosome movement throughout the nucleus is apparent in many zygotene cells, whereas chromosomes in cells at pachynema appear to move less expansively, with only subtle motions of the cores being observed. Some cells exhibit no chromosome movement at all, possibly related to the viability of the cell. Individual AEs/LEs, particularly the larger, brighter telomeric ends of chromosomes, can be tracked over time as we have done with the red, blue, and yellow chromosome clusters in Figure 9. Additionally, chromosomes appear to join telomere clusters and then to disengage from these clusters over time, which can be seen in the movies and also the blue telomere cluster in Figure 9; this starts out with three clearly visible telomeres but as the imaging period progresses only two telomeres can be seen (Supplementary Movies S6–S10, Figure 9). This demonstrates that chromosome movement in mouse spermatocytes is much more subtle than the dramatic chromosome movements and rearrangements observed in yeast (Scherthan *et al*. 2007). This may be due to the difference in the portion of the meiotic cycle covered during the observation time in mice versus yeast. Additionally, these chromosome movements are consistent with the rotations and oscillations observed by Parvinen & Soderstrom (1976), including their observation that the most active movements are at zygonema and movement progressively slows down through pachynema.

Okadaic acid induced progression from pachynema to diplonema can be observed in live spermatocytes

OA, a phosphatase inhibitor, induces precocious entry into metaphase I in cells that are competent to undergo chromosome condensation (Cobb *et al*. 1999). Progression from pachynema to diplonema/diakinesis occurs in a matter of hours, rather than days, making it feasible to observe this transition *in vitro*. Similar to published reports (Wiltshire *et al*. 1995), fluorescent spermatocytes treated with OA for 6 h and imaged before (Figure 10c,e,g) and after treatment (Figure 10d,f,h) show appropriate progression from pachynema to diakinesis. However, the OA-induced prophase I progression described in previous studies (Wiltshire *et al*. 1995) is not normal and SC breakdown is aberrant. This is consistent with our findings. For example, see Figure 10b, where a very strong, punctate staining pattern for SYCP3 is seen along both the X and Y chromosomes, where it

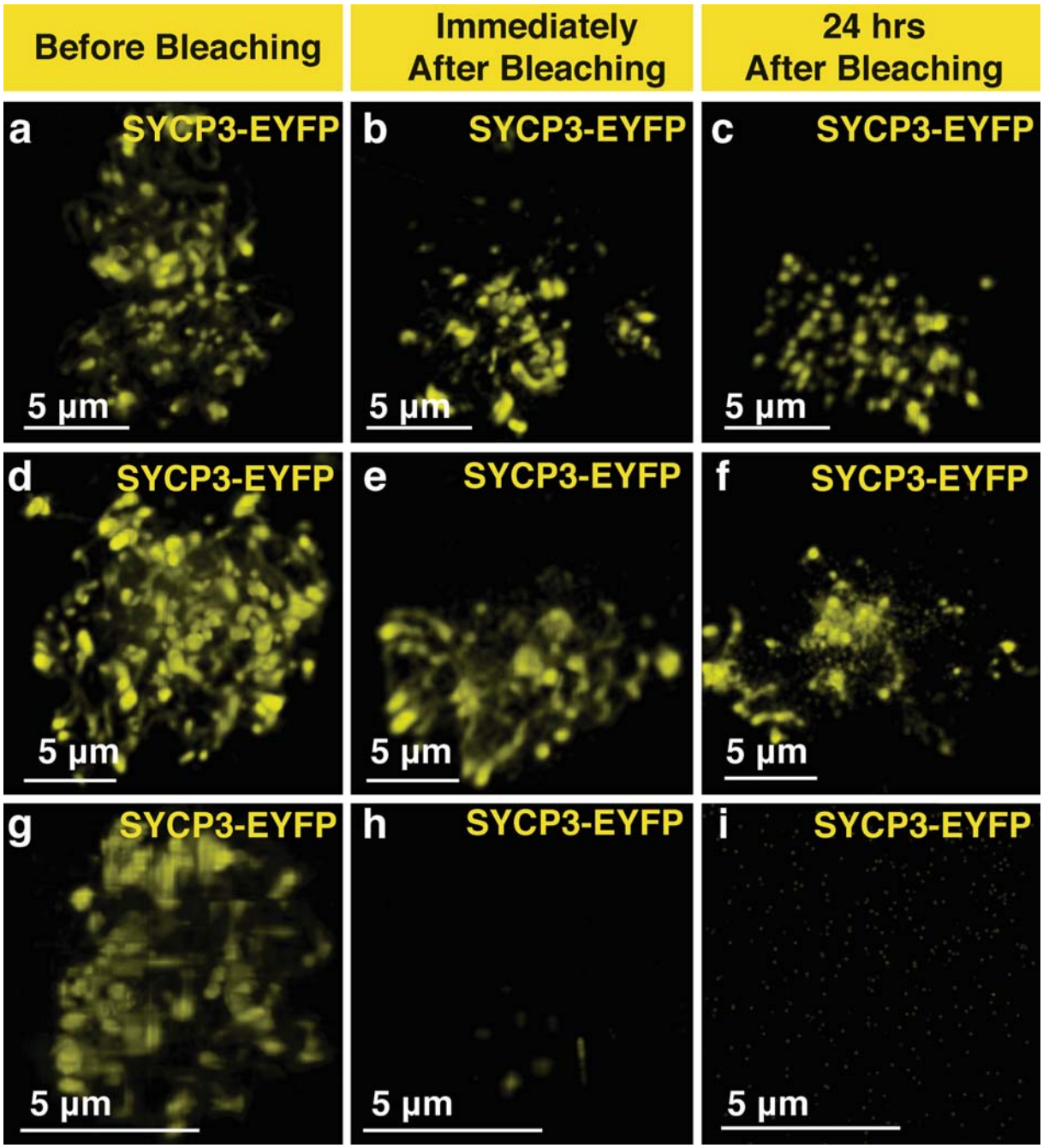

Figure 8. Fluorescence recovery after photobleaching. (**a**, **d**, **g**) 3D renderings of z-stack images of three different spermatocytes, most likely in late pachytene or early diplotene, imaged in the YFP channel. (**b**, **e**, **h**) Images of the same spermatocytes immediately after photobleaching. (**c**, **f**, **i**) Images of the same spermatocytes 24 h after photobleaching. Scale bars represent 5 μm.

persists after the rest of the SCs are broken down, consistent with previous reports (Tarsounas *et al*. 1999). In live OA-treated spermatoctyes this same punctate pattern can be seen in SYCP3–EYFP fluorescence (Figure 10d,f,h). Progression from pachynema to diakinesis can also be seen occurring over time via time-lapse imaging of fluorescent spermatocytes (Supplementary Movies S11 and

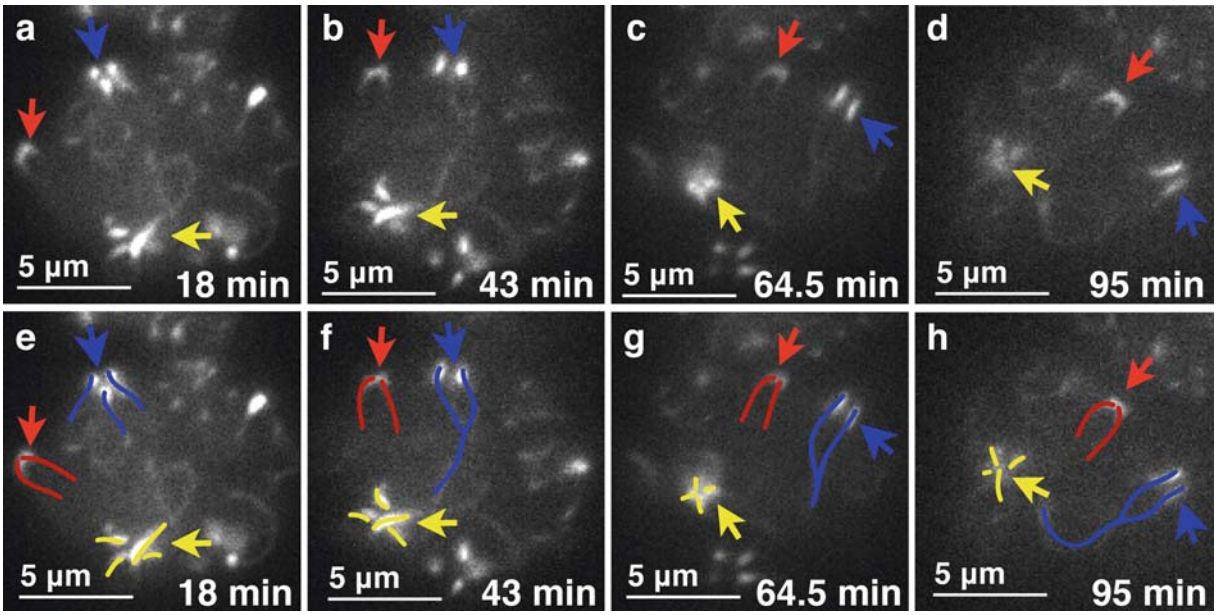

Figure 9. Tracking of chromosomes in a diplotene *Sycp3–Eyfp*^{21HC} spermatocyte. (**a**–**d**) Four frames taken from a time-lapse image of a spermatocyte over 180 min. The arrows point to telomere clusters that can be tracked as they move around the nucleus over the period of imaging. (**e**–**h**) The same four frames with the tracked chromosomes traced, each cluster in a different color. The time point at which each frame is captured is given in minutes on panels (e)–(h). The entire time-lapse movie can be viewed in Supplementary Movie S6. Scale bars represent 5 μm.

S12). Thus, meiotic progression, albeit drug-induced, can be observed in live fluorescent cells.

Discussion

The current study introduces a live-imaging system for viewing meiosis in live mouse spermatocytes and provides proof-of-principle evidence to support the use of such a system for assessing meiotic progression. *Sycp3–Eyfp*^{21HC} mice are viable and fertile, indicating that transgene expression does not interfere with meiotic progression. However, while the SYCP3–EYFP protein is expressed in the expected testis-specific manner and localizes to AEs/LEs as expected, transgene expression does not rescue the *Sycp3* null phenotype. This may be due to inadequate transgene expression, although subtle defects in SYCP3 function cannot be ruled out. Additionally, transgene function may be compromised by the altered expression pattern driven by the PGK2 promoter, the lack of posttranslational or transcriptional modifications that occur on endogenous SYCP3, or interference by the EYFP tag. In this study the PGK2 promoter was chosen because of its demonstrated ability to drive transgene expression in mice (Robinson *et al*. 1989, Zhang *et al*. 1999). Finally, transgene expression may be dependent, at least partially, on the existence of endogenous SYCP3, which is under the regulation of the endogenous *Sycp3* promoter and is thus expressed under appropriately regulated conditions.

Staging criteria for *Sycp3–Eyfp*^{21HC} spermatocytes developed in this study have been based on the state of AE/LE formation/dissolution and pairing/unpairing as well as heterochromatin localization and telomere clustering, which have all been well characterized previously and can be discerned from 3D images of Hoechst-stained *Sycp3–Eyfp*^{21HC} spermatocytes. Unfortunately, the percentage of fluorescent nuclei that can be staged is low and is biased toward pachytene nuclei, which have the brightest fluorescence. This is due to a relatively weak signal that photobleaches quickly and has a negligible turnover rate, resulting in no recovery of fluorescence after photobleaching and restricting our ability to re-image individual cells over long periods. These difficulties aside, the current study demonstrates our

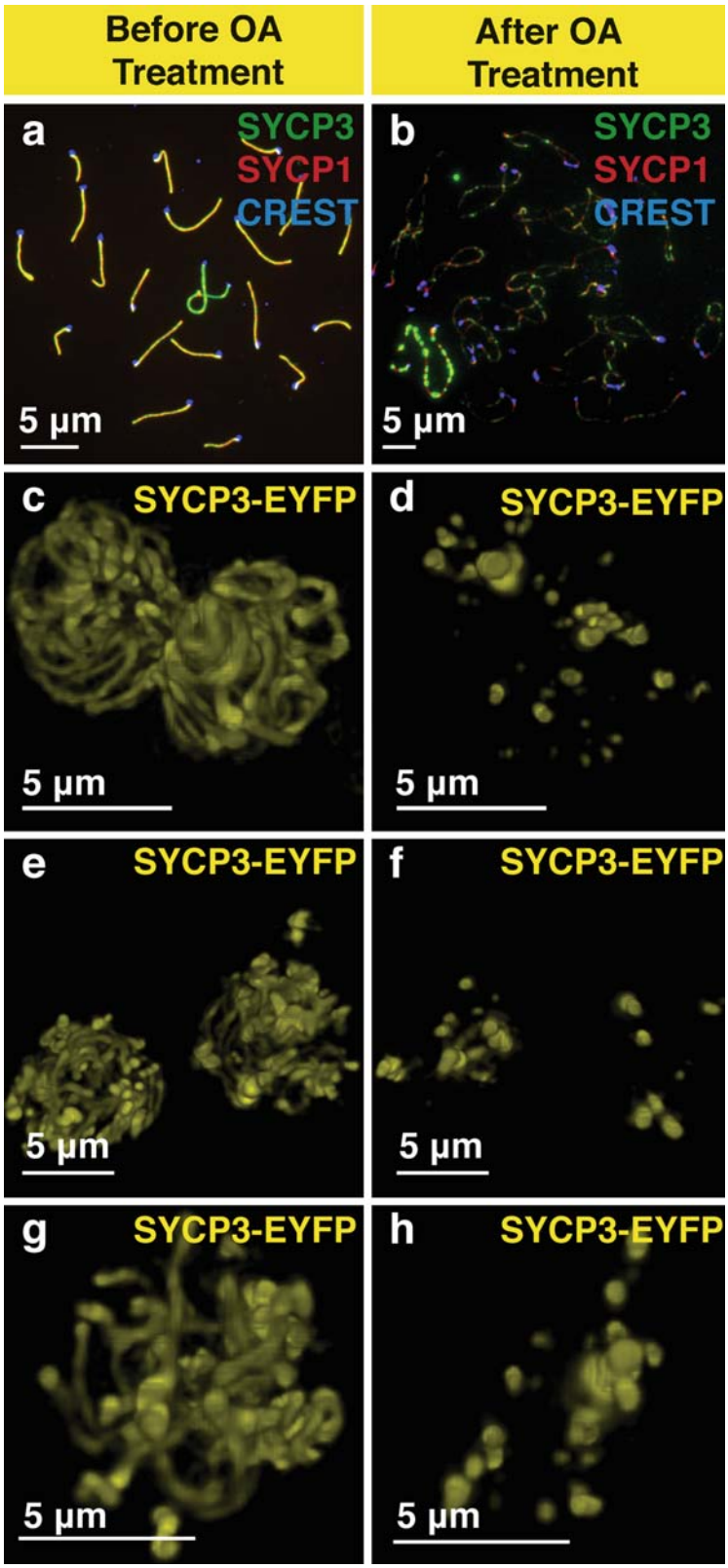
Before OA Treatment
After OA Treatment
a
SYCP3
SYCP1
CREST
5 μm
b
SYCP3
SYCP1
CREST
5 μm
c
SYCP3-EYFP
5 μm
d
SYCP3-EYFP
5 μm
e
SYCP3-EYFP
5 μm
f
SYCP3-EYFP
5 μm
g
SYCP3-EYFP
5 μm
h
SYCP3-EYFP
5 μm

◀*Figure 10*. Meiotic progression from pachynema to diplonema of OA-treated *Sycp3–Eyfp*^{21HC} spermatocytes. (**a**) A meiotic spread of an untreated pachytene spermatocyte stained for SYCP3 (green), SYCP1 (red), and CREST (blue). (**b**) A meiotic spread of a spermatocyte, stained the same as (a), after 6 h of treatment with OA. (**c**, **e**, **g**) 3D renderings of z-stack images taken in the YFP channel of spermatocytes before OA treatment. (**d**, **f**, **h**) The same spermatocytes after 6 h of OA treatment. Scale bars equal 5 μm.

ability to stage nuclei, track AEs/LEs through the nucleus, observe telomere clustering, and observe chromosome movement, all while keeping the cell alive. These are all useful analytical tools that could be applied to the study of meiotic mutants, such as those with pairing defects, or after manipulating the nuclei in different ways (protein synthesis inhibition, microtubule inhibition).

Our findings on telomere clustering and distribution in prophase I substages are largely consistent with previous results (Scherthan *et al*. 1996) and the minor differences in the number of telomere clusters and heterochromatic regions observed in certain stages, especially early prophase I, may be due to the nature of the imaging, the inherent subjectivity involved, and/or the use of different criteria.

Using this system, aspects of the 3D architecture of spermatoctyes can be observed that would not be possible with current techniques. For example, the XY body is known to be separate from the rest of the nucleus (Handel 2004), and this can be readily observed in 3D images of spermatocytes (Figure 6). In addition, residual SYCP3–EYFP fragments remaining at the centromeres in diakinesis can occasionally be observed in an ordered conformation (Figure 6), possibly due to the chromosomes lining up in preparation for the first meiotic division.

This system becomes more powerful with the ability to image the same spermatocyte multiple times in culture. Previous studies have used detection of SC proteins by western blotting as evidence of meiotic progression (Hubner *et al*. 2003), but SC components may no longer be localized correctly and/or associated with an intact chromosomal core. Observation of live fluorescent AEs/LEs during the duration of an experiment would provide a reliable measure of spermatocyte viability in culture. Although photobleaching makes true time-lapse imaging difficult in 3D, manipulation of the imaging protocol has allowed the same spermatocyte to be imaged in 3D several times over the course of an experiment. As proof-of-principle, OA-treated spermatocytes have been imaged in 3D before and after treatment and OA-induced progression to diplonema and diakinesis is observed.

The ability to track chromosome movement in real time during meiosis has been lacking in most model organisms, with the exception of yeast (White *et al*. 2004). Scherthan *et al*. examined the dynamics of yeast meiosis with a ZIP1::GFP fusion strain and were able to monitor and characterize AE/LE movements during prophase I and observe meiotic progression (Scherthan *et al*. 2007). Studies such as these have proved to be much harder to perform in mice. However, imaging in a single focal plane makes it possible to monitor spermatocytes over the course of an experiment up to 2 h long, and in the current study we demonstrate that mouse meiocytes can be visualized in short-term culture scenarios and chromosome movement can be observed. We find that chromosome movement in mouse spermatocytes is quite subtle and generally involves the chromosome ends moving around in relation to the rest of the chromosome compared to the dramatic chromosomes movement of entire chromosomes and nuclear rearrangements observed in yeast. This is perhaps not unexpected as yeasts undergo meiosis at a much faster rate than mice.

In summary, the *Sycp3–Eyfp*^{21HC} mouse offers researchers a tool to visualize prophase I events in 4D, and could be applied to many meiotic studies including genetic or chemically induced meiotic mutants. Future studies could expand the utility of this mouse model by co-expressing other fluorescent fusion constructs or by creating a knock-in version of the Sycp3–Eyfp model to fully complement the *Sycp3* null mutation.

Acknowledgements

This work was supported by funding from the NIH to P.E.C. (HD41012). *Sycp3* nullizygous mice were kindly provided by Dr Christer Hoog (Karolinska Institut, Sweden). The SMC3 antibody was kindly provided by Dr Rolf Jessberger (Institute of Biochemistry and Molecular Cell Biology, Technical University, Dresden, Germany). We thank Ross LaRosa and George Lunney of Carl Zeiss MicroImaging Inc. for their generous and unceasing assistance with imaging.

References

Bass HW, Marshall WF, Sedat JW, Agard DA & Cande WZ (1997) Telomeres cluster de novo before the initiation of synapsis: a three-dimensional sparial analysis of telomere positions before and during meiotic prophase. *J Cell Biol* **127**: 5–18.

Cobb J, Cargile B & Handel MA (1999) Acquisition of competence to condense metaphase I chromosomes during spermatogenesis. *Dev Biol* **205**: 49–64.

Eijpe M, Offenberg H, Jessberger R, Revenkova E & Heyting C (2003) Meiotic cohesin REC8 marks the axial elements of rat synaptonemal complexes before cohesins SMC1beta and SMC3. *J Cell Biol* **160**: 657–670.

Handel M (2004) The XY body: a specialized meiotic chromatin domain. *Exp Cell Res* **296**: 57–63.

Hassold T, Sherman S & Hunt PA (1995) The origin of trisomy in humans. *Prog Clin Biol Res* **393**: 1–12.

Hassold T, Abruzzo M, Adkins K *et al*. (1996) Human aneuploidy: incidence, origin, and etiology. *Environ Mol Mutagen* **28**: 167–175.

Hassold T & Hunt P (2001) To err (meiotically) is human: the genesis of human aneuploidy. *Nat Rev Genet* **2**: 280–291.

Hubner K, Furhmann G, Christenson L *et al*. (2003) Derivation of oocytes from mouse embryonic stem cells. *Science* **300**: 1251–1256.

Hunt P, Lemaire R, Embury P, Sheean L & Mroz K (1995) Analysis of chromosome behavior in intact mammalian oocytes: monitoring the segregation of a univalent chromosome during female meiosis. *Hum Mol Genet* **4**: 2007–2012.

Kolas N, Marcon E, Spyropoulos B & Moens PB (2005a) Mutant meiotic chromosome core components in mice can cause an apparent sexual dimorphic endpoint at prophase or X-Y defective male specific sterility. *Chromosoma* **114**: 92–102.

Kolas NK, Svetlanov A, Lenzi ML *et al*. (2005b) Localization of MMR proteins on meiotic chromosomes in mice indicates distinct functions during prophase I. *J Cell Biol* **171**: 447–458.

Lammers JH, Offenberg HH, Van Aalderen M, Vink AC, Dietrich AJ & Heyting C (1994) The gene encoding a major component of the lateral elements of synaptonemal complexes of the rat is related to X-linked lymphocyte-regulated genes. *Mol Cell Biol* **14**: 1137–1146.

Liu L, Franco S, Spyropoulos B, Moens PB, Blasco MA & Keefe DL (2004) Irregular telomeres impair meiotic synapsis and recombination in mice. *Proc Natl Acad Sci U S A* **101**: 6496–6501.

McCarrey JR, Berg WM, Paragioudakis SJ *et al*. (1992) Differential transcription of Pgk genes during spermatogenesis in the mouse. *Dev Biol* **154**: 160–168.

Moens PB & Spyropoulos B (1995) Immunocytology of chiasmata and chromosomal disjunction at mouse meiosis. *Chromosoma* **104**: 175–182.

Page SL & Hawley RS (2004) The genetics and molecular biology of the synaptonemal complex. *Annu Rev Cell Dev Biol* **20**: 525–558.

Parvinen M & Soderstrom K-O (1976) Chromosome Rotation and formation of synapsis. *Nature* **260**: 534–535.

Pelttari J, Hoja MR, Yuan L *et al*. (2001) A meiotic chromosomal core consisting of cohesin complex proteins recruits DNA recombination proteins and promotes synapsis in the absen23e of an axial element in mammalian meiotic cells. *Mol Cell Biol* **21**: 5667–5677.

Peters AH, Plug AW, Van Vugt MJ & De Boer P (1997) A drying-down technique for the spreading of mammalian meiocytes from the male and female germline. *Chromosome Res* **5**: 66–68.

Robinson MO, Mccarrey JR & Simon MI (1989) Transcriptional regulatory regions of testis-specific PGK2 defined in transgenic mice. *Proc Natl Acad Sci U S A* **86**: 8437–8441.

Scherthan H (2007) Telomere attachment and clustering during meiosis. *Cell Mol Life Sci* **64**: 117–124.

Scherthan H, Weich S, Schwegler H, Heyting C, Harle M & Cremer T (1996) Centromere and telomere movements during early meiotic prophase of mouse and man are associated with the onset of chromosome pairing. *J Cell Biol* **134**: 1109–1125.

Scherthan H, Jerratsch M, Li B *et al*. (2000) Mammalian meiotic telomeres: protein composition and redistribution in relation to nuclear pores. *Mol Biol Cell* **11**: 4189–4203.

Scherthan H, Wang H, Adelfalk C *et al*. (2007) Chromosome mobility during meiotic prophase in *Saccharomyces cerevisiae*. *Proc Natl Acad Sci U S A* **104**: 16934–16939.

Tanemura K, Ogura A, Cheong C *et al*. (2005) Dynamic rearrangement of telomeres during spermatogenesis in mice. *Dev Biol* 196–207.

Tarsounas M, Pearlman, RE & Moens PB (1999) Meiotic activation of rat pachytene spermatocytes with okadaic acid: the behaviour of synaptonemal complex components SYN1/SCP1 and COR1/SCP3. *J Cell Sci* **112**: 423–434.

Thomas KH, Wilkie TM, Tomashefsky P, Bellve AR & Simon MI (1989) Differential gene expression during mouse spermatogenesis. *Biol Reprod* **41**: 729–739.

Trelles-Sticken E, Dresser ME & Scherthan H (2000) Meiotic telomere protein Ndj1p is required for meiosis-specific telomere distribution, bouquet formation and efficient homologue pairing. *J Cell Biol* **151**: 95–106.

White EJ, Cowan C, Cande WZ & Kaback DB (2004) *In vivo* analysis of synaptonemal complex formation during yeast meiosis. *Genetics* **167**: 51–63.

Wiltshire T, Park C, Caldwell KA & Handel MA (1995) Induced premature G2/M-phase transition in pachytene spermatocytes includes events unique to meiosis. *Dev Biol* **169**: 557–567.

Yuan L, Liu JG, Zhao J, Brundell E, Daneholt B & Hoog C (2000) The murine SCP3 gene is required for synaptonemal complex assembly, chromosome synapsis, and male fertility. *Mol Cell* **5**: 73–83.

Zhang LP, Stroud J, Eddy CA, Walter CA & Mccarrey JR (1999) Multiple elements influence transcriptional regulation from the human testis-specific PGK2 promoter in transgenic mice. *Biol Reprod* **60**: 1329–1337.

Zickler D & Kleckner N (1998) The leptotene–zygotene transition of meiosis. *Annu Rev Genet* **32**: 619–697.

Zickler D & Kleckner N (1999) Meiotic chromosomes: integrating structure and function. *Annu Rev Genet* **33**: 603–754.